arXiv:1512.01583v1 [physics.plasm-ph] 4 Dec 2015

Transonic ablation flow regimes of high-Z pellets

Hyoungkeun Kim[1], **Roman Samulyak**[1,2], **Paul Parks**[3]
[1] *Department of Applied Mathematics and Statistics, Stony Brook University, Stony Brook, NY 11794*
[2] *Computational Science Center, Brookhaven National Laboratory, Upton, NY 11973*
[3] *General Atomics, P.O. Box 85608, San Diego, California 92186-5608*

July 15, 2014

The injection of cryogenic pellets for plasma refueling is the method of choice for future reactor-scale tokamaks such as ITER [1]. One-dimensional, spherically-symmetric, quasi-steady state models such the transonic flow model [2] have provided scaling laws and successfully predicted pellet ablation rates and penetration depths. Theoretical work has been complemented by two-dimensional numerical simulations that resolved detailed physics processes in the ablation cloud [5], including the MHD effects [6, 7]. Previous studies, focusing on the fueling application of pellets, have limited the choice of the pellet material to deuterium. However high-Z pellets have a great potential for other important tokamak applications, in particular the plasma disruption mitigation. In this letter, we report results of numerical studies of the ablation of argon and neon pellets and compare them with theoretical predictions and studies of deuterium pellets. Simulations have been performed in the spherically-symmetric approximation using the hydrodynamic / MHD code FronTier [8] with recently developed physics models for the pellet ablation such as the electronic heat flux model and the numerical equation-of-state (EOS) with the support for multiple ionization of high-Z gases [14]. The code has been extencively used for simulations of phase transitions [9], high power mercury target experiments [10, 11]. An overview of application problems is given in [12].

The main equations for the pellet ablation cloud are the inviscid Euler

equations with external heat source:

$$\frac{\partial \rho}{\partial t} = -\nabla \cdot (\rho \mathbf{u}), \tag{1}$$

$$\rho \left(\frac{\partial}{\partial t} + \mathbf{u} \cdot \nabla \right) \mathbf{u} = -\nabla P, \tag{2}$$

$$\rho \left(\frac{\partial}{\partial t} + \mathbf{u} \cdot \nabla \right) e = -P \nabla \cdot \mathbf{u} - \nabla \cdot \mathbf{q}, \tag{3}$$

$$P = P(\rho, e) \tag{4}$$

where ρ, $\mathbf{u}$, e, and P are density, velocity, specific internal energy, and pressure, respectively. The term $(-\nabla \cdot \mathbf{q})$ described the external heat source of hot electrons streaming along magnetic field line into the ablation cloud.

As details of transonic regimes of the pellet ablation flow are strongly dependent on atomic physics processes in the ablation cloud, the quality of numerical equation of state models describing partially ionized plasmas is of significant importance. While probabilities of multiply ionized states in high-Z materials in the local thermodynamic equilibrium is accurately described by coupled system of Saha equations [13], the direct use of these equations in time-dependent hydrodynamic simulations is prohibitively computationally intensive. In our previous works [14, 15], we have developed a numerical EOS model for argon based on the Zel′dovich approximation of average ionization [13]. The average ionization model (AIM) relates the average ionization level $\overline{m}$ with the thermodynamic states as $\overline{m} = \frac{AT^{3/2}}{n} \exp -\frac{\overline{I}}{kT}$ and computes the pressure as $P = (1 + \overline{m})\rho RT$. This model is sufficiently accurate in the high energy regime. However, as it is shown in Figure 1, the accuracy is reduced at low temperatures corresponding to the average ionization level of order ($\overline{m} \sim 0.1$). The ablation cloud near the pellet surface is in weakly ionized state, and the inaccuracy of the original AIM could change the overall dynamics of ablation cloud in simulations. In this work, we improve our previous numerical EOS for high-Z gases by including the linear continuum approximation of statistical weight ratio ($\overline{u}$) shown in Figure 2. The equation in the improved AIM with $\overline{u}$ is:

$$\overline{m} = \overline{u}\ \frac{AT^{3/2}}{n} \exp -\frac{\overline{I}}{kT}. \tag{5}$$

The accuracy of this numerical EOS is increased further by using the numerical optimization of $\overline{I}$ when $\overline{m} < 1$. We use the modified $\overline{I}$ instead of the linear approximation to mimic the single electron model in the low energy regime. In this work, $\overline{I} = I_1(1 - \overline{m}^q)^{1/q}$ is used, where I_1 is the first

ionization energy and q is a properly picked rational number when $\overline{m} < 1$. The result of the improved AIM is shown in the Figure 1.

We compare simulations of high-Z gases with molecular deuterium described in [5, 6, 7]. The equation of state model for deuterium that accounts for dissociation and ionization uses the exact system of Saha equations. We also compare our results with simulations obtained using the polytropic EOS model that defines the gas pressure as $P = (\gamma - 1)\rho e$, where γ is the ratio of specific heats.

The electron heat flux model is identical to that of the previous works [3, 5, 6, 7] except the modification of the Coulomb logarithm and the dimensionless opacity for high-Z atoms. The modified Coulomb logarithm is:

$$\ln \Lambda = \frac{\overline{m}}{Z} \ln \Lambda_{ef} + \frac{(1 - \overline{m})}{Z} \ln \Lambda_{eb}$$

in which Z=atomic number, $\Lambda_{ef} = 0.2E/\hbar\omega_{pe}, \omega_{pe} = (4\pi n_e e^2/m_e)^{1/2}$, $\Lambda_{eb} = E/I_* \sqrt{e/2}$, $E \approx 2T_{e\infty}$(plasma electron temperature), n_e=plasma electron density, and I_* is the mean excitation energy (for example, $I_*^H = 19.2$ eV, $I_*^{Ne} = 137$ eV, and $I_*^{Ar} = 188$ eV from [4]). The changed dimensionless opacity in the spherically symmetric approximation is $u = \tau/\tau_{eff}$, where

$$\tau(r) = Z \int_r^\infty n(r')dr', \qquad \tau_{eff} = \tau_\infty \sqrt{\tfrac{2}{1+Z}}, \qquad \tau_\infty = \tfrac{T_{e\infty}^2}{8\pi e^4 \ln \Lambda}.$$

The pellet surface ablation model is identical to that of [6] with the exception of some technical improvements, namely the numerical treatment of high gradients of physics quantities near the pellet surface.

We start with the simulation of a deuterium pellet using parameters of [6], namely the pellet radius of $r_p = 0.2cm$, the plasma electron temperature of $T_{e\infty} = 2keV$, and the plasma electron density of $n_{e\infty} = 10^{14} cm^{-3}$. Simulations with the polytropic EOS demonstrate a transonic ablation flow that starts as subsonic near the pellet surface and changes to supersonic due to the electron heat flux (Figure 3(a)). When the deuterium plasma EOS is used (Figure 3(b)), the ablation flow is affected by energy sinks due to the dissociation and ionization. The dissociation processes slow down the increase of the Mach number near the pellet surface. The flow accelerates then to supersonic velocities before the majority ionization processes occur. The ionization energy causes the shock wave and the drop of the Mach number below unity. The flow then accelerates again and reached the supersonic state the second time (double transonic pellet ablation regime). The temperature T^* and pressure P^* of the ablation cloud at the sonic radius r^* are shown in Table 1. The ablation rate using polytropic EOS in

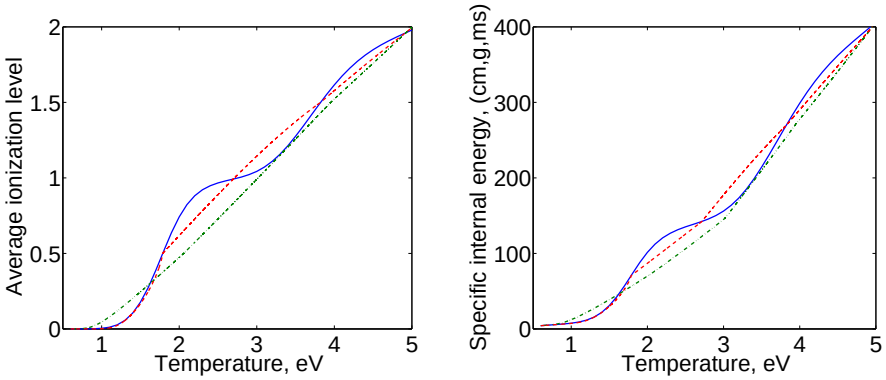

(a) Average ionization (b) Specific internal energy

Figure 1: The comparison of solutions from the coupled system of Saha equations (solid blue line), the original average ionization model (green dash-dotted line), and the improved average ionization model (red dashed line) for neon with density of $3.351 \times 10^{-5}\ g/cm^3$.

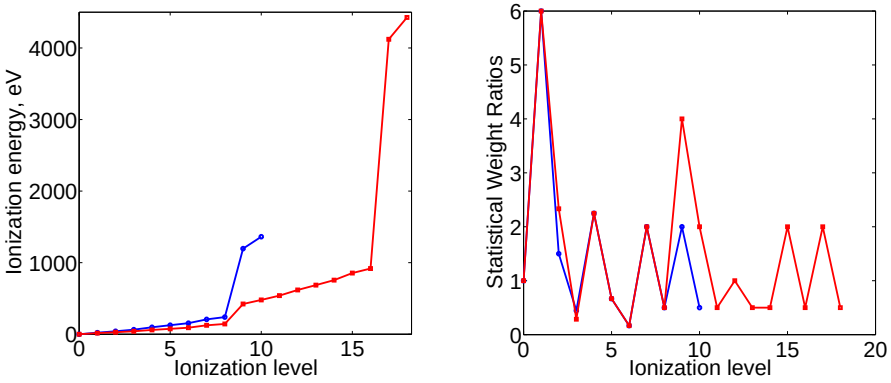

(a) Ionization energy, $\overline{I}$ (b) Statistical weight ratios, $\overline{u}$

Figure 2: Ionization energy and statistical weight ratios of neon (blue-circle) and argon (red-square)

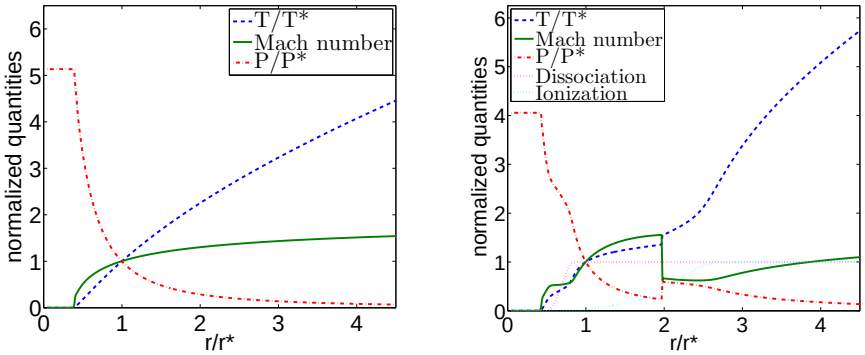

(a) Polytropic EOS (b) Plasma EOS

Figure 3: Normalized ablated cloud profiles of deuterium pellet in 1-dimensional spherically symmetric model of ablation (a) without atomic processes (polytropic EOS), and (b) with atomic processes (plasma EOS).

Table 1 is consistent with the value of 133 g/s predicted by the theoretical transonic flow model of [2]. The ablation rate is reduced by approximately 10.7% when the atomic processes are included in the EOS.

	r* (cm)	T* (eV)	P* (bar)	Ablation rate (g/s)
Polytropic EOS ($\gamma = 7/5$)	0.518	3.21	29.25	132.6
Plasma EOS	0.474	1.04	25.54	118.4

Table 1: The ablated cloud states of deuterium pellet at the first sonic radius (r*) for the cases with polytropic EOS and plasma EOS.

	r* (cm)	T* (eV)	P* (bar)	$\overline{m}$*	Ablation rate (g/s)
Polytropic EOS ($\gamma = 5/3$)	0.603	30.15	22.96	-	112.9
Plasma EOS	0.603	4.84	16.37	1.99	95.3

Table 2: The ablated cloud states of neon pellet at the first sonic radius (r*) for the cases with polytropic EOS and plasma EOS.

In the pellet ablation simulation of neon and argon, the states of ablation cloud at sonic radius is shown in the table 2 and 3 and the normalized quan-

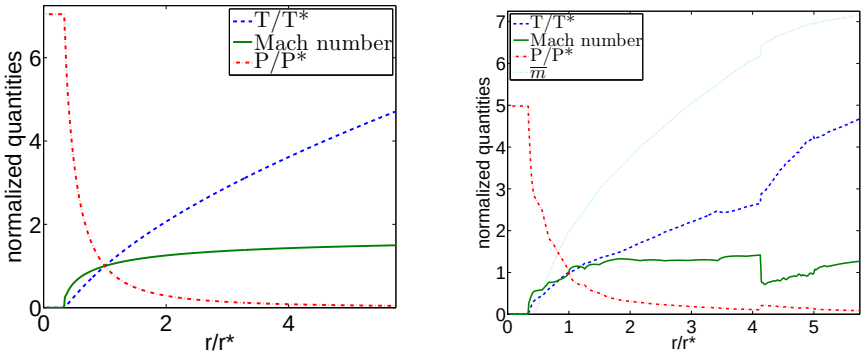

(a) Polytropic EOS (b) Plasma EOS

Figure 4: Normalized ablated cloud profiles of neon pellet in 1-dimensional spherically symmetric model of ablation (a) without atomic processes (polytropic EOS), and (b) with atomic processes (plasma EOS).

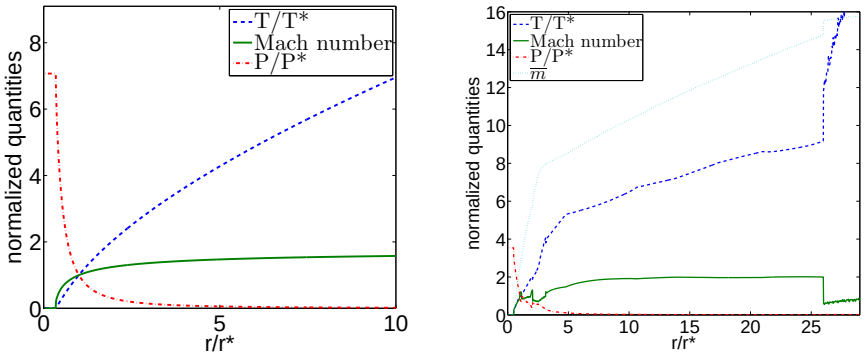

(a) Polytropic EOS (b) Plasma EOS

Figure 5: Normalized ablated cloud profiles of argon pellet in 1-dimensional spherically symmetric model of ablation (a) without atomic processes (polytropic EOS), and (b) with atomic processes (plasma EOS).

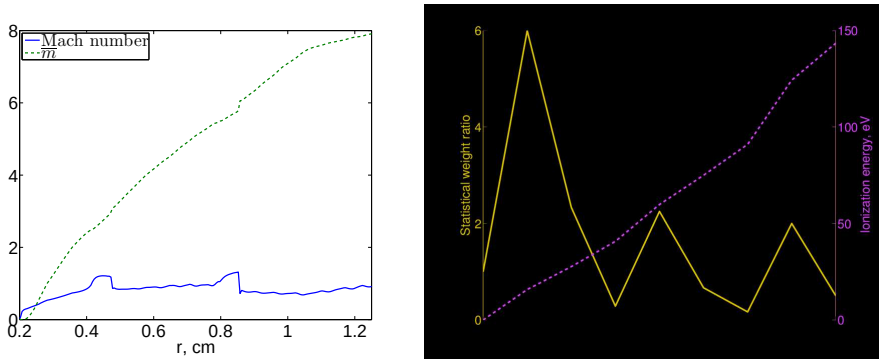

(a) Ablation flow of argon pellet (b) Atomic property of argon

Figure 6: The local property of argon pellet's ablation flow near the pellet surface (a) and the corresponding atomic property of argon (b).

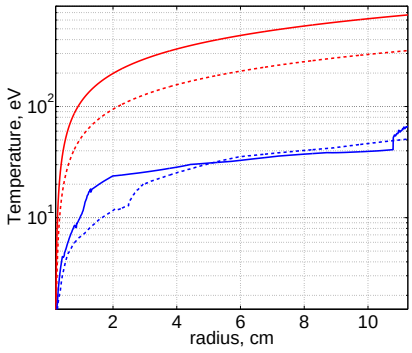

Figure 7: The comparison of ablated gas temperature of neon pellet (dashed line) and argon pellet (solid line) with polytropic EOS (red line) and plasma EOS (blue line)

	r* (cm)	T* (eV)	P* (bar)	$\overline{m}$*	Ablation rate (g/s)
Polytropic EOS ($\gamma = 5/3$)	0.588	61.82	22.62	-	103.6
Plasma EOS	0.415	4.46	20.04	2.49	77.4

Table 3: The ablated cloud states of argon pellet at the first sonic radius (r*) for the cases with polytropic EOS and plasma EOS.

tities based on them are provided in Figures 4 and 5. For simulations that neglect ionization using the polytropic EOS, the ablation rates in Tables 2 and 3 are in reasonably good comparison to the theoretical predictions of 109 g/s for neon and 103 g/s for argon using the transonic flow model [2]. The ablation flow of the neon pellet exhibits the double transonic regime similar to the deuterium case. Slowly increasing ionization potentials of the neon atom corresponding to the ionization levels from 1 to 8 irregularly reduce the ablation flow acceleration and cause oscillations on the Mach number plot in Figure 4(b). Despite these energy sinks, the flow accelerated above the sonic point. Then the large increase of the ionization energy associated with stripping off the 9th and 10th electrons drop the Mach number below unity and cause the shock wave. Then the flow again reaches the supersonic state.

The ablation flow regime is more complex for the argon pellets (Figure 5(b)). The ionization energy of the argon atom slowly increases with the increase of the ionization level from 1 to 16, with the exception of a bigger change of the ionization potential between levels 8 and 9 (see Figure 2(a)). Nevertheless, the Mach number twice drops below unity before the average ionization reaches level 6 (see Figure 6 that shows details of the Mach number and the average ionization close to the pellet surface). This is caused by the combination of the increasing ionization energy with statistical weights that rapidly increase for the ionization level 3 and 6 (see Figure 6(b)), causing the weak shock waves in the ablation flow. Then the flow slowly and steadily accelerates under constant energy removal by ionization. When the ionization level reaches 16, the rapid increase of the ionization potential between levels 16 and 17 causes the third shock wave. Then the flow of fully ionized argon accelerates again above the sonic point.

A large reduction of temperature in the neon and argon pellet simulations with real gas EOS compared to the polytropic gas simulations can be understood via consecutive ionization energy losses. For the argon pellet, there is one order of magnitude difference of temperature at the first sonic

radius (table 3) and this difference is consistently observed along the ablation cloud, as shown in the Figure 7. The reductions of the ablation rates for the neon and argon pellets by atomic processes, $\sim 15.6\%$ and $\sim 25.3\%$ respectively, is significantly larger compared to the case of deuterium pellets. The reason for this is well understood in terms of ionization energy losses.

References

[1] B Pgouri. Review: Pellet injection experiments and modelling. Plasma Phys. and Controlled Fusion, 49, R87, 2007.

[2] P. B. Parks, R. J. Turnbull. Effect of transonic flow in the ablation cloud on the lifetime of a solid hydrogen pellet in a plasma. *Phys. Fluids*, 21:1735, 1978.

[3] P. B. Parks, W. D. Sessions, L. R. Baylor. Radial displacement of pellet ablation material in tokamaks due to the grad-B effect. *Phys. Plasmas*, 5:1968, 2000.

[4] ICRU Report 37, Stopping powers and ranges for protons and alpha particles. *International Commission of Radiation Units and Measurement*, 1984.

[5] R. Ishizaki, P. B. Parks, N. Nakajima, M. Okamoto. Two-dimensional simulation of pellet ablation with atomic processes. *Phys. Plasmas*, 11:4064, 2004.

[6] R. Samulyak, T. Lu, and P. Parks. A magnetohydromagnetic simulation of pellet ablation in electrostatic approximation. *Nuclear Fusion*, 47:103–118, 2007.

[7] P. Parks, T. Lu, and R. Samulyak. Charging and $E \times B$ rotation of ablation clouds surrounding refueling pellets in hot fusion plasmas. *Phys. Plasmas*, 16:060705, 2009.

[8] R. Samulyak, J. Du, J. Glimm, Z. Xu, A numerical algorithm for MHD of free surface flows at low magnetic Reynolds numbers, J. Comp. Phys., 226 (2007), 1532 - 1549.

[9] S. Wang, R. Samulyak, T. Guo, An embedded boundary method for parabolic problems with interfaces and application to multi-material systems with phase transitions, Acta Mathematica Scientia, 30B (2010), No. 2, 499 - 521.

[10] A. Hassanein at el., An R&D program for targetry and capture at a neutrino factory and muon collider source, Nuclear Instruments and Methods in Physics Research Section A: Accelerators, Spectrometers, Detectors and Associated Equipment, 501 (1), 70 - 77.

[11] R. Samulyak, Y. Prykarpatskyy, T. Lu, J. Glimm, Z. Xu, M.-N. Kim, Comparison of heterogeneous and homogenized numerical models of cavitation, International Journal for Multiscale Computational Engineering, 4 (2006), No 3, 377 - 389.

[12] B. Fix, J. Glimm, X. Li, Y. Li, X. Liu, R. Samulyak, Z. Xu, A TSTT integrated FronTier code and its applications in computational fluid physics, Journal of Physics: Conference Series, 16 (2005), 471 - 475.

[13] Ya. B. Zel′dovich and Yu. P. Raizer. *Physics of shock waves and high-temperature hydrodynamic phenomena*. Dover, 2002.

[14] H. Kim, R. Samulyak, L. Zhang, P. Parks. Influence of atomic processes on the implosion of plasma liners. *Phys. Plasmas*, 19:082711, 2012.

[15] H. Kim, L. Zhang, R. Samulyak, P. Parks. "On the Structure of Plasma Liners for Plasma Jet Induced Magnetoinertial Fusion," *Phys. Plasmas*, 20:022704 ,2013.